Astron. Astrophys. 320, 929–944 (1997)

ASTRONOMY
AND
ASTROPHYSICS

Interstellar CH^+ in southern OB associations

Roland Gredel[1]

[1] European Southern Observatory, Casilla 19001, Santiago 19, Chile (rgredel@eso.org)

Received 6 June 1996 / Accepted 1 October 1996

Abstract. Optical absorption line observations of interstellar CH^+ and CH are presented towards the southern OB associations CMa OB1, NGC 2439, Vela OB1, NGC 4755, and Cen OB1. A total of 5–11 stars per association were observed, with visual extinctions ranging from A_V = 0.5–4.5 mag. The derived CH^+ and CH velocities agree within the measurement errors. Towards a particular association, the CH^+ column density $N(CH^+)$ is correlated to the visual extinction of the background star. These findings weaken the possibility that magnetic shocks are the general mechanism that is required to produce interstellar CH^+. It is found that $N(CH^+)$ is correlated to $N(CH)$, which indicates that $N(CH^+)$ is correlated to the optical depth of a cloud. The correlations are difficult to reconcile with scenarios where the sites of CH^+ formation are constrained to the surface of molecular clouds. The observations support ideas which involve turbulence as a major CH^+ production mechanism. In particular, the results are in agreement with expectations from a scenario where the CH^+ formation proceeds in cool gas via a fraction of fast, non-Maxwellian H_2 or C^+, created by the dissipation of interstellar turbulence.

Key words: ISM: abundances – ISM: clouds – ISM: molecules – open clusters and associations

1. Introduction

In his review of the problems related to the formation of interstellar CH^+, D. A. Williams (1992) concluded that 'it is our understanding of the interstellar medium that is inadequate, rather than our knowledge of chemistry'. The CH^+ problem arises because the molecule is rapidly destroyed by reactions with H and H_2, and models of quiescent molecular clouds predict CH^+ column densities that are orders of magnitude below the observed values. The commonly adopted way to elevate the modeled CH^+ column densities to the levels observed in the interstellar medium is to propel its formation rate via the exchange reaction $C^+ + H_2 \rightarrow CH^+ + H$. This reaction is endothermic by 4650 K (0.4 eV) and thus requires the presence of disturbances upon the quiescent gas. Among the suggestions that have been made are shocks (Elitzur & Watson 1978, 1980), photoelectric heating of the gas in strong radiation fields (White 1984b), formation via a fraction of translationally hot H_2 (Lambert & Danks 1986), boundary layers heated by turbulence (Duley et al. 1992), and transiently heated layers of hot gas from intermittent dissipation of interstellar turbulence (Falgarone et al. 1995).

The observational evidence in favor of the shock hypothesis is inconclusive. A controversial result concerns the presence of a velocity shift between CH^+ and the CH, which is expected from magnetic shock models. While a number of studies concluded that velocity shifts are in general absent (e.g. Lambert & Danks 1989, Crawford 1989, Lambert et al. 1990, Hawkins & Craig 1991, Gredel et al. 1993), others found significant velocity shifts (e.g. Allen & Snow 1992, Penprase 1993, Allen 1994). In some cases, discrepancies exist for the same light of sight. Towards the sightlines studied at very high spectral resolution (Lambert et al. 1990, Crane et al. 1995, Crawford 1995), the velocity shifts are small in general. There are other dependences of the CH^+ column density $N(CH^+)$ on observable parameters which can be compared with the expectations from the various CH^+ formation scenarios. It is generally found that towards randomly oriented lines of sight, $N(CH^+)$ increases with the visual extinction A_V of the background star (e.g. Penprase 1993, Gredel et al. 1993). Whether this is an argument in favor or against the shock models is not clear, however, as towards random lines of sight, a large value of A_V often reflects a large distance to the background star. The larger CH^+ columns may thus be produced by more than one intercepting shock. From a comparison of CH^+ and C_2 observations, Gredel et al. (1993) found evidence that $N(CH^+)$ decreases with the gas density n. Although C_2 and CH^+ may not reside entirely in the same parcels of gas, the trend in the $N(CH^+)$ - n relation may nevertheless indicate that the CH^+ formation is enhanced in low density regions.

It is the aim of the present work to investigate if a $N(CH^+)$-A_V correlation holds for an individual cloud as well, and if $N(CH^+)$ is correlated to the optical depth of the cloud. To avoid the distance ambiguity, observations were obtained towards various members of an OB association. The stars in a given association are known to be at similar distances. Changes in A_V may thus be related to changes in the optical depth of the foreground 'cloud', more so if the radial velocities inferred

Send offprint requests to: R. Gredel

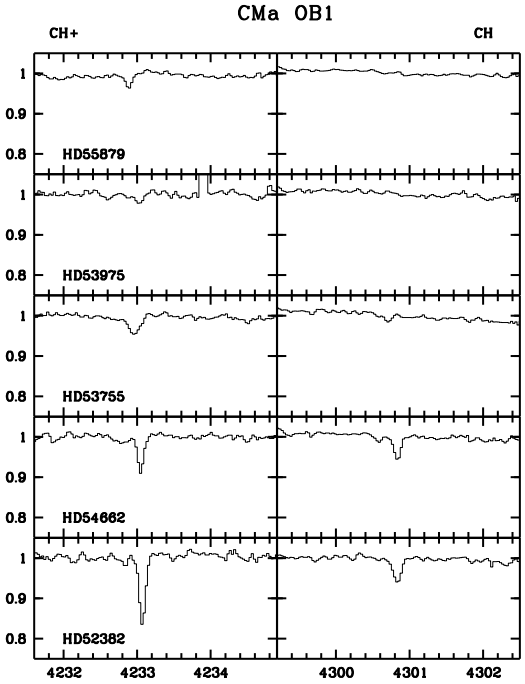

Fig. 1. Spectra of the interstellar CH^+ $A^1\Pi$–$X^1\Sigma^+$ (0,0) line around 4232 Å and of the CH $A^2\Delta$–$X^2\Pi$ (0,0) line around 4300 Å towards stars in CMa OB1. Continua are normalized to 1. Spectra are rebinned to a linear, heliocentric wavelength scale $\lambda_{\rm hel}$. Stars are identified in the CH^+ spectra

towards the various lines of sight are similar (see however the discussion in Scalo 1990). In the following, CH^+ and CH observations are presented towards the southern OB associations CMa OB1, the association surrounding NGC 2439, Vela OB1, NGC 4755, and Cen OB1. Spectra are obtained towards 5–11 stars per association, with visual extinctions ranging from 0.5–4.5 mag. The observational results are summarized in Sects. 2 and 3 below. A comparison of the results with the predictions from shock models is given in Sect. 4.1. A detailed linear regression analysis of the data is presented in Sect. 4.2, together with a discussion of the statistical significance of the correlations in Sect. 4.3. Section 4.4 concludes with a comparison of the observational results with expectations from models which involve CH^+ formation in photon-dominated regions, in turbulent boundary layers of molecular clouds, in low density regions which are transiently heated by the dissipation of turbulence, and in cold regions where a fraction of fast but non-Maxwellian H_2 or C^+ is created via the interstellar turbulence. The conclusions of the present work are summarized in Sect. 5.

2. Observations and reduction

Interstellar CH^+ absorption lines which arise in the R(0) line of the (0,0) and (1,0) bands of the $A^1\Pi$-$X^1\Sigma^+$ system, near 4232 Å and near 3957 Å, respectively, were observed with the ESO Coudé Echelle Spectrograph (CES) at the 1.4m Coudé Auxiliary Telescope (CAT). A total of 33 stars in the southern OB associations CMa OB1, the association surrounding NGC 2439, Vela OB1, NGC 4755, and Cen OB1, were observed, with values of $A_{\rm V}$ ranging from 0.5–4.5 mag. The CH^+ observations were complemented by observations of the CH $R_{2e}(1) + R_{2f}(1)$ Λ-doublet in the (0,0) band of the $A^2\Delta$-$X^2\Pi$ system, near 4300 Å. A few additional spectra were obtained covering the $Q_2(1)$+ $^QR_{12}(1)$ blend near 3886 Å and the $^PQ_{12}(1)$ line near 3890 Å, which arise in the (0,0) band of the $B^2\Sigma^-$-$X^2\Pi$ system. The CES resolution was set to R=$\lambda/\Delta\lambda$ = 70000. Typical exposure times were 0.5–2 hours per star, depending on its apparent magnitude. This resulted in a signal-to-noise ratio (S/N) of typically S/N$\geq$ 50 in most spectra. The observations were performed in March 1993, November 1993 and in March 1994 using the ESO CCD #9 as detector. The individual CCD frames were dark and bias subtracted, flat fielded, and rebinned to a linear, heliocentric wavelength scale. Gaussian fits to individual spectra should provide velocities accurate to $<$1/3 pixels or $<$ 0.7 km s^{-1} excluding systematic errors. The accuracy of the final wavelength scale is estimated to be of the order of 1–2 km s^{-1} . Spectra of six stars were measured in January 1996 using the ESO Multi Mode Instrument (EMMI) at the ESO New Technology Telescope (NTT). EMMI was configured with echelle #14 and grism #5 as cross disperser, which resulted in a spectral coverage of 4000–6500 Å at a resolution of R$\approx$ 80000. The ESO CCD#34 was used as detector. The integration time per star was 30 min. The CAT and the EMMI data were reduced employing the ESO 'Munich Image Data Analysis System' MIDAS (e.g. Banse et al. 1983).

3. Results

The following four subsections 3.1–3.4 summarize the measurements obtained here. Tables 1–4 list the observational results obtained with the CES, and Tab. 5 contains the results obtained with EMMI. Each table identifies the stars and their visual extinction $A_{\rm V}$ (in mag) in columns 1 and 2, respectively. Visual extinctions are adopted from Humphreys (1978). Columns 3–6 list the heliocentric wavelengths in Å , the inferred heliocentric velocities in km s^{-1} , the measured equivalent widths W_λ in mÅ , and the derived column densities N in units of 10^{13} cm^{-2}, respectively. The molecular parameters given in Gredel et al. (1993) (their table 2) were employed to infer column densities and velocities. For CH^+, column densities in $N(0)$ are tabulated, and for CH, those in the $N'' = 1, J'' = 1/2$ level are given. The 3886Å and 3890Å CH lines that arise in the (0,0) band of the $B^2\Sigma^-$-$X^2\Pi$ system originate in one Λ doublet only, and the corresponding column densities given in Tabs. 1–4 have been multiplied by a factor of 2.

The equivalent widths measured here are large in general and a curve of growth analysis is necessary to infer column densities. This requires the knowledge of the Doppler-b value and a knowledge of the number of absorbing components along the line of sight. In principle, the Doppler b-value in the line forming region can be determined from observations of saturated and unsaturated absorption lines that arise from the same

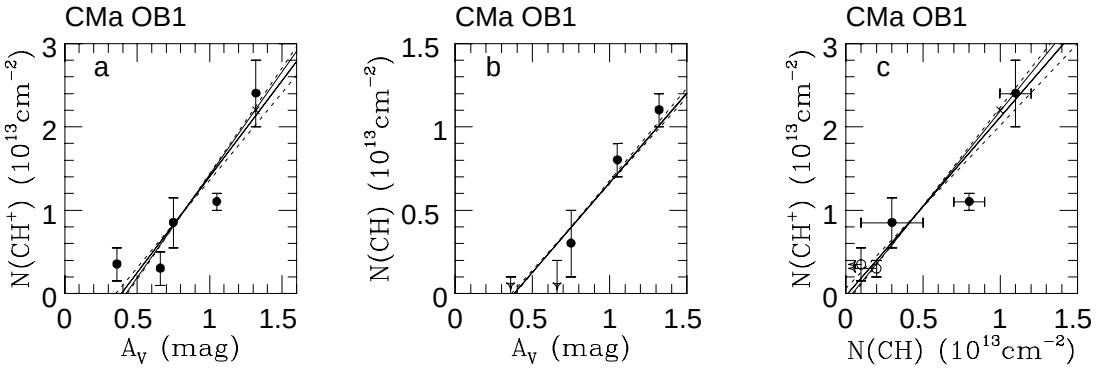

Fig. 2a–c. Total CH$^+$ and CH column densities plotted as a function of the visual extinction A_V (**a,b**) towards CMa OB1. **c** CH$^+$ column densities plotted vs CH column densities. Dashed and full lines represent linear regressions fitted to the data (see text)

upper level. In the present case, a comparison of the CH A-X (4300 Å) and the CH B-X (3886 or 3890 Å) lines may be used to obtain the CH Doppler b value b(CH). The CH B-X (3886 Å) line was measured towards one star in each association. The comparison suggests b-values of $b \approx 1.5$–2 km s^{-1} for HD 61827, $b \approx 1.5$–2 km s^{-1} for CPD–32° 1734, $b = 1$–1.5 km s^{-1} towards HD 75860, and b=1.5–2 km s^{-1} for CPD–45°3218. These values are larger than the Doppler-b values inferred by Gredel et al. (1991, 1993) towards other stars in NGC 2439 and in Vela, namely $b = 0.4$–0.9 km s^{-1} for HD 63804 in NGC 2439 and $b = 0.6$–1.7 km s^{-1} for HD 73882 in Vela OB1. The latter values were inferred from CO and CN, and may not be appropriate to infer b(CH), more so if CH is more widespread than e.g. CN (Federman et al. 1994). It is also not clear to what fraction CH coexists with CH$^+$ in a possibly warm gas, in which case b(CH) = b(CH$^+$) may be adopted, both for pure thermal broadening and for pure turbulent broadening (see however the discussion in Gredel et al. (1993), their section 5). The average value of b(CH) inferred by Crawford (1995) and by Crane et al. (1995) from the resolved line profiles is of the order of 1.5 km s^{-1} . Lacking a more accurate determination of b(CH) towards most of the stars observed here, a value of b(CH)=1.5 km s^{-1} is applied in an undiscriminated way to derive the saturation corrections for CH. The Λ-doubling of the CH 4300 line was treated explicitly in the curve of growth calculation (see Gredel et al. 1993). The CH column densities corrected for saturation effects are listed in column 7 of Tabs. 1–5. Values are only given if the saturation corrections exceed the error margins on N(CH) in the limit $b \rightarrow \infty$. For CH$^+$, a comparison of the R(0) lines that arise in the (1,0) and (0,0) bands, respectively, provides in principle the CH$^+$ Doppler-b value. However, as already noticed by Gredel et al. (1993), the difference in oscillator strength between that line pair is small, and measurement uncertainties prevent a reliable determination of b(CH$^+$). The saturation corrections for CH$^+$ are here estimated using b(CH$^+$) = 2–3 km s^{-1} , which appears to be a typical value for CH$^+$. Similar values are suggested from the resolved line profiles obtained by Lambert et al. (1990), Hawkins & Craig (1991), Crawford (1995), and Crane et al. (1995). The CH$^+$ column densities corrected for saturation are listed in column 7 of Tabs. 1–5.

The following sections include plots of the CH$^+$ and the CH column densities versus A_V , and of N(CH$^+$) versus N(CH). In each diagram, various linear regressions fitted to the data points are given. The two dashed lines correspond to ordinary least squares (OLS) fits minimizing the residuals in X and in Y, respectively, and the full lines correspond to the orthogonal regression line, the OLS bisector, and the reduced major-axis. The various regressions are discussed in detail in Sect. 4.2.

3.1. CMa OB1

The CMa OB1 association has been studied in detail by Clariá (1974), who inferred a photometric distance of 1150 pc and a total to selective absorption ratio of R = A_V / E_{B-V} = 3.0 ± 0.6. Radio continuum observations (Nakano et al. 1984) suggest that CMa OB1 is associated with an old supernova remnant (SNR).

The individual spectra of the CH$^+$ 4232 Å and the CH 4300 Å lines are shown in Fig. 1, arranged in such a way that the visual extinction A_V of the stars increases from the top to the bottom. Figs. 2a-c are plots of N(CH$^+$) vs. A_V , N(CH) vs. A_V , and of N(CH$^+$) vs. N(CH), respectively. Column densities corrected for saturation effects are used. The saturation corrections reach about 10% for HD 52382 for CH$^+$ and CH but are of minor nature for the rest of the data. The crosses in Figs. 2a-c represent CH$^+$ and CH column densities towards HD 52382 inferred in the limit $b \rightarrow \infty$.

The CH column density in the velocity component near 18 km s^{-1} seen towards HD 54662 is not considered in Figs. 2b,c. The dashed and full lines in the three diagrams represent the various regressions fitted to the data points, see Sect. 4.2 for a discussion. Both N(CH$^+$) and N(CH) are correlated to A_V , and N(CH$^+$) is correlated to N(CH), as will be shown in Sect. 4.3.

Towards HD 52382 and HD 54662, the CH$^+$ and CH velocities agree within ≈ 1 km s^{-1} (cf. Tab. 1). The measurements towards HD 53755 indicate a velocity shift of ≈ 3 km s^{-1} but the line/continuum ratio is very low, which prevents an accurate determination of velocities. The other stars in CMa OB1 have no CH detections. A number of additional measurements towards HD 54662 are available from the literature. Lambert & Danks (1986) measured an equivalent width of W_λ(4232 Å) =

Table 1. CH$^+$ and CH measurements towards CMa OB1[a]

Star	A_V	λ_{hel}	V_{hel}	W_λ	N_∞	N_b
HD55879	0.36	4232.89	24.2	3.5(2.0)	0.4(.2)	
		3958.00	23.3	1.5(1.5)	0.3(.3)	
		4300.66	24:	≤ 1	≤ 0.1	
HD53975	0.66	4233.02	33.4	3.0(2.5)	0.3(.2)	
		4300.79	33:	≤ 2	≤ 0.2	
HD53755	0.75	4232.96	29.1	9.0(1.5)	1.0(.2)	
		3958.10	30.9	3.0(1.0)	0.7(.2)	
		4300.70	26.9	2.5(2.0)	0.3(.2)	
HD54662	1.05	4233.05	35.5	9.5(1.0)	1.1(.1)	
		4300.58	18.6	1.5(0.5)	0.2(.1)	
		4300.83	36.0	6.5(0.5)	0.8(.1)	
HD52382	1.32	4233.07	36.9	18.0(1.5)	2.1(.2)	2.3
		3958.19	37.7	10.8(1.0)	2.4(.2)	2.5
		4300.83	36.0	8.0(1.0)	1.0(.1)	1.1

[a] see text for units

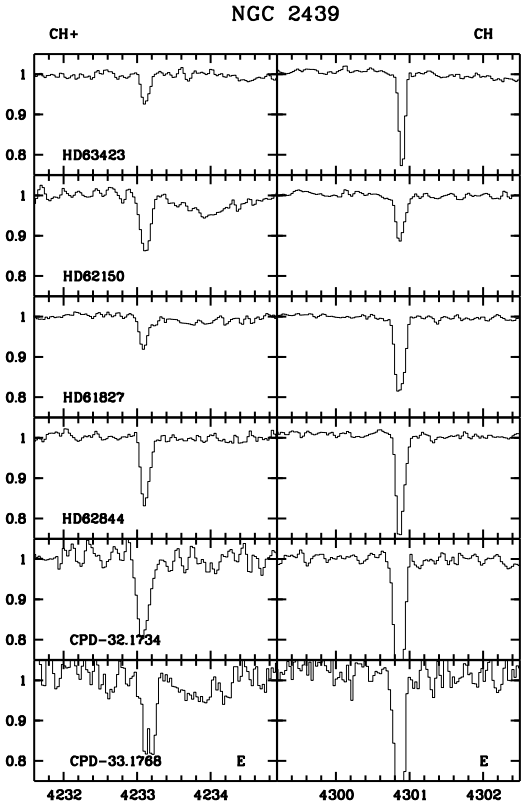

Fig. 3. CH$^+$ and CH spectra towards stars in the association surrounding NGC 2439. Label E identifies spectra taken with EMMI

9.7 ± 0.5 mÅ at a radial velocity of V_{hel} = +34 km s^{-1} , in good agreement with the values reported here, $W_\lambda = 9.5 \pm 1.0$ mÅ at V_{hel} = +35.5 km s^{-1} . For CH, Danks et al. (1984) obtained values of W_λ(4300 Å) = 2.0 $\pm$ 0.7 mÅ and 7.3 $\pm$ 0.7 mÅ for two CH velocities components near 18 km s^{-1} and 33 km s^{-1} , respectively, compared to values of 1.5 $\pm$ 0.5 mÅ and 6.5 $\pm$ 0.5 mÅ near 18.6 km s^{-1} and 36 km s^{-1} , respectively, found here. There is only marginal agreement in the CH velocities. Allen (1994) measured velocities of 31.7 km s^{-1} and 35.5 km s^{-1} for CH$^+$ and CH, respectively. The corresponding value of $\Delta V \approx 4$ km s^{-1} for the CH$^+$ - CH velocity shift is in discrepancy with the value of $\Delta V < 1$ km s^{-1} obtained here. Allen (1994) did not report the detection of the weaker CH component near 18 km s^{-1} .

Table 2. CH$^+$ and CH measurements towards NGC 2439[a]

Star	A_V	λ_{hel}	V_{hel}	W_λ	N_∞	N_b
HD63423	1.53	4233.10	39.1	9.0(1.0)	1.0(.1)	1.1
		3958.22	39.9	5.0(2.0)	1.1(.4)	1.1
		4300.90	40.8	23.5(0.5)	2.8(.1)	3.5
HD62150	1.77	4233.11	39.7	23.0(2.0)	2.7(.2)	3.1
		3958.22	39.9	10.7(1.0)	2.3(.2)	2.5
		4300.87	38.8	17.0(1.5)	2.1(.2)	2.4
HD61827	2.10	4233.09	38.3	10.0(1.0)	1.2(.1)	1.3
		4300.87	38.8	30.0(1.0)	3.6(.1)	4.8
		3886.91	38.6	9.5(1.5)	4.4(.7)	4.9
HD62844	2.67	4233.11	39.7	24.0(1.5)	2.8(.2)	3.2
		4300.88	39.5	34.0(3.0)	4.1(.4)	5.7
–32°1734	3.66	4233.09	38.3	37.0(3.0)	4.3(.3)	5.5
		4300.86	38.1	53.5(3.0)	6.5(.4)	12
		3886.91	38.6	20.0(2.0)	9.4(.9)	12

[a] see text for units

3.2. The association surrounding NGC 2439

The stars in the association surrounding NGC 2439 are closely associated in age and distance to NGC 2439 itself, as shown by Turner (1977). The distance to the cluster was given by White (1975) as 3.4 kpc. One star, HD 61827, shows a peculiar ultraviolet extinction curve (Meyer & Savage 1981).

Table 2 lists the CAT observations towards five stars in the association. Additional data on CPD–33°1768, measured with EMMI, are given in Tab. 5. Visual extinctions of the stars range from A_V = 1.5–4.5 mag. The individual spectra obtained for CH$^+$ (4232) and for CH (4300) are shown in Fig. 3, arranged from top to bottom with increasing A_V . Spectra obtained with EMMI are labeled 'E'. At the resolution employed here, the CH$^+$ and the CH absorption lines do not split up into multiple velocity components. Fig. 4a-b plot CH$^+$ and CH column densities corrected for saturation versus visual extinction A_V , and Fig. 4c plots N(CH$^+$) versus N(CH). Crosses represent column densities inferred in the limit $b \rightarrow \infty$. Dashed and full lines show various linear regression lines fitted to the data points, see Sect. 4.2 for a discussion. Figs. 4a-c include the CH$^+$ and CH column densities towards the additional member HD 63804, taken from Gredel et al. (1993). Both the CH and the CH$^+$ column densities are correlated to A_V , and N(CH$^+$) is correlated to N(CH), as will be shown in Sect. 4.3.

The CES and EMMI data towards CPD–32°1734 agree well with each other, cf. Tabs. 2 and 5. The 50% discrepancy in N(CH) inferred from the 3886Å line and from the 4300Å line towards CPD–32°1734 indicates that the 4300Å line is strongly saturated. The CH$^+$ and the CH lines towards CPD–32°1734 were measured simultaneously with EMMI, which ensures that the CH$^+$-CH velocity difference is not affected by systematic

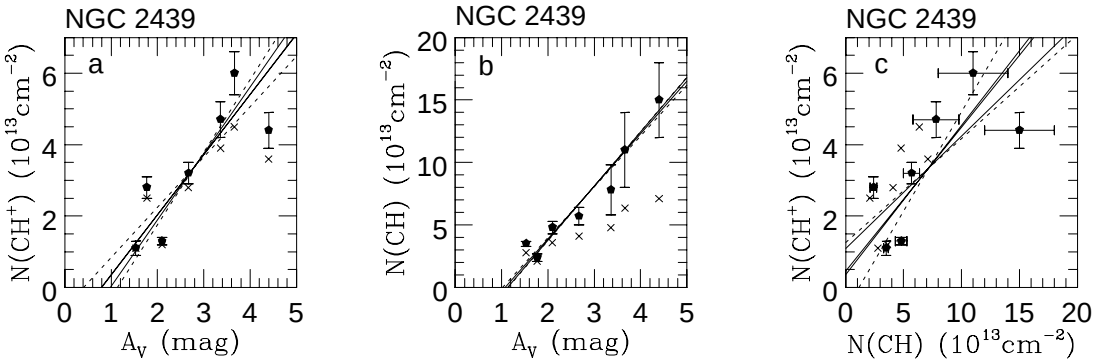

Fig. 4a–c. NGC 2439: Total CH$^+$ and CH column densities plotted versus visual extinction A_V (**a, b**) and CH$^+$ column density plotted versus that of CH (**c**). Crosses represent column densities not corrected for saturation. Dashed and full lines represent linear regressions fitted to the data (see text)

Table 3. CH$^+$ and CH measurements towards Vela OB1[a]

Star	A_V	λ_{hel}	V_{hel}	W_λ	N_∞	N_b
HD78344	4.20	4232.83	20.0	24.0(1.0)	2.8(.1)	3.2
		3957.99	22.5	17.0(2.0)	3.7(.4)	4.1
		4300.59	19.3	50.0(3.0)	6.0(.4)	10.5
HD74371	0.93	4232.88	23.5	11.5(2.0)	1.3(.2)	1.4
		4300.64	22.8	8.0(1.0)	1.0(.1)	1.0
HD75149	1.14	4232.89	24.2	10.0(1.0)	1.2(.1)	1.2
		4300.66	24.2	14.5(0.5)	1.8(.1)	2.0
HD74194	1.62	4232.83	20.0	13.5(3.5)	1.6(.4)	1.7
		4300.63	22.1	10.0(1.0)	1.2(.1)	1.3
HD75211	2.16	4232.90	24.9	26.5(1.0)	3.1(.1)	3.6
		3958.00	23.3	15.5(1.0)	3.4(.2)	3.6
		4300.65	23.4	19.0(1.0)	2.3(.1)	2.7
HD76556	2.19	4232.60	3.7	14.0(1.0)	1.6(.1)	1.8
		3957.75	4.4	5.0(1.5)	1.1(.3)	1.1
		4300.34	1.9	28.0(2.5)	3.4(.3)	4.4
HD75860	2.79	4232.85	21.4	48.0(1.0)	5.6(.1)	7.8
		3957.98	21.8	27.0(1.0)	5.9(.2)	7.1
		4300.61	20.7	18.5(1.0)	2.2(.1)	2.6
		3886.67	20.1	7.0(2.0)	3.3(.9)	3.6
–45°3218	3.18	4232.86	22.1	21.0(3.0)	2.4(.3)	2.8
		4300.63	22.1	45.5(2.0)	5.5(.2)	9.0
		3886.69	21.6	10.0(2.0)	4.7(.9)	5.3
		3890.51	22.5	16.0(3.0)	11(2.2)	13.5
–46°3272	3.18	4232.86	22.1	24.0(3.0)	2.8(.3)	3.2
		4300.62	21.4	39.5(2.0)	4.8(.2)	7.1

[a] see text for units

errors. Velocity differences are $<$ 1 km s^{-1} measured with EMMI and with the CES. The CH$^+$ and CH velocities towards the other stars agree within the errors, with the exception of CPD–33°1768, where the velocities disagree by about 5 km s^{-1} . The line profiles towards the latter star deviate from single Gaussians, and both spectra suffer from a low S/N, with S/N $<$ 30, two factors which affect the inferred velocities. Because of the low S/N, no attempt was made to fit multiple Gaussians to the spectra.

3.3. Vela OB1

A number of OB associations are located in the direction of the Vela SNR and the Gum Nebula (e.g. Slawson & Reed 1988), and a considerable amount ultraviolet and optical absorption line observations are available towards many sight lines in this region. Most studies have focused on bright stars with low reddening, $E_{B-V} < 0.5$ mag. They reveal the presence of highly ionized material indicating shock excitation (e.g. Jenkins et al. 1984 and references therein), with shock velocities in the 50–100 km s^{-1} range (e.g. Wallerstein & Balick 1990). Relatively high CH$^+$ columns are seen towards a few stars in the direction of the Vela SNR (Wallerstein & Gilroy 1992). Optical and ultraviolet absorption line observations towards the binary HD 72172 reveal spatial and temporal changes in the absorption line profiles (Wallerstein et al. 1995 and references therein). A number of sightlines show absorption components at very high velocities (Wallerstein & Silk 1971, Jenkins et al. 1984), which indicates the presence of chaotic motions towards the Vela SNR.

The observations presented here focus on the Vela OB1 association. Its average distance of 1.9 kpc (Humphreys 1978) places the entire association well behind the Gum Nebula and the Vela SNR. Vela OB1 is located towards the Vela Molecular Ridge (VMR), which has been identified through millimeter CO observations (Murphy & May 1991). Kinematic distances to the CO clouds range from 1–2 kpc (Murphy & May 1991). The reddening towards Vela OB1 is low up to a distance of some 1kpc (Eggen 1980, 1982). (NB: Note that the notation adopted to identify the different associations in Vela is not unique; the most distant association, Vela OB1 here, is named Vela OB2 in other publications).

Table 3 summarizes the present CAT measurements, with the corresponding CH$^+$ (4232) and CH(4300) spectra shown in Fig. 5. Measurements towards CPD–44°3129 obtained with EMMI are given in Tab. 5, corresponding spectra are labeled 'E' in Fig. 5. The spectrum on top of Fig. 5 correspond to HD 78344, which is not a member of Vela OB1 but is located in the same part of the sky than other members of Vela OB1, at a distance of 1.7 kpc (as listed in van Dishoeck & Black

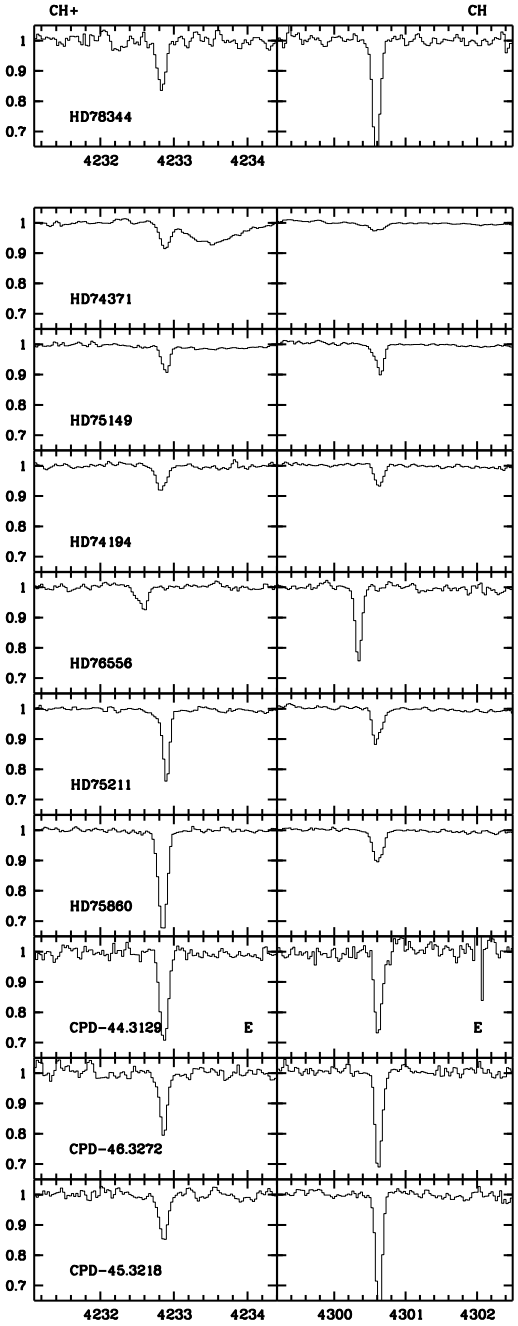

Fig. 5. Vela OB1: CH^+ and CH spectra towards individual stars. Label E identifies spectra taken with EMMI

1989). Other spectra are arranged with increasing visual extinction from the top to the bottom. The inferred CH^+ and CH velocities towards most of the stars in Vela OB1 agree well within the measurement errors. Towards three sightlines, a velocity difference of the order of 2 km s^{-1} is inferred, but the corresponding spectra suffer from either a low S/N (HD 78344), or the line profiles deviate from single Gaussians (HD 74194 and HD 76556), two factors which may affect the inferred velocities.

Figs. 6a–c show plots of $N(CH^+)$ and $N(CH)$ versus A_V and of $N(CH^+)$ versus $N(CH)$. Crosses represent data not corrected for saturation effects. Dashed and full lines represent various linear regressions, see Sect. 4.2. The figure includes the CH^+ and CH column densities obtained towards HD 73882 by Gredel et al. (1993). The CH^+ and CH column densities are correlated to the visual extinction, as shown in Sect. 4.3. Note that the star with the highest CH^+ column density, HD 75860, is probably associated with the HII region RCW 75.

Previous observations towards HD 75149 (Danks et al. 1984) resulted in a CH equivalent width of $W_\lambda(4300)$ of 14.3 $\pm$ 0.6 mÅ at V_{hel} = 21.3 km s^{-1} , compared to 14.5 $\pm$ 0.5 mÅ at V_{hel} = 24.2 km s^{-1} obtained here. Molecular carbon towards HD 78344 was observed near V_{hel} (C_2) = 25 $\pm$ 3 km s^{-1} (van Dishoeck & Black 1989). The radial velocities towards the observed stars in Vela OB1 are all within the range of V_{hel} = 19–25 km s^{-1} , which compares well with the CO velocities of V_{hel} = 22–26 km s^{-1} of CO in the VMR (Murphy & May 1991). This may suggest that the CH and CH^+ absorptions arise in the VMR itself. The Vela SNR is located at distances less than 1 kpc, and probably at a distance of $<<$ 500 pc (Jenkins & Wallerstein 1995). It is thus not expected that the molecular material in the VMR is affected by interactions with the SNR. Towards HD 75194, Danks & Sembach (1996) inferred the presence of very high velocity gas seen in CaII, with CaII velocities ranging from V_{hel} = –125 km s^{-1} to –45 km s^{-1} . The NaI profiles indicate velocities in the –1.5 km s^{-1} to +28 km s^{-1} range. As it is the case for HD 72172, the atomic absorption lines show temporal variations. The spectra towards HD 75149 obtained here do not reveal CH^+ or CH absorption lines at the very high velocities of CaII.

3.4. NGC 4755 and Cen OB1

The compact southern galactic cluster NGC 4755 (κ Crucis or Herschel's Jewel Box), is located at a distance of 2.2–2.3 kpc and has a mean interstellar reddening of E_{B-V} = 0.44 mag (Dachs & Kaiser 1984, Kaltcheva & Georgiev 1994). The measurements of E_{B-V} towards the various stars in NGC 4755 by Dachs & Kaiser (1984) and by Kaltcheva & Georgiev (1994) differ by up to 10%. Five stars in NGC 4755 were studied here, with visual extinction ranging from A_V = 1.0–1.4 mag (Humphreys 1978). Spectra were obtained towards additional stars in the Cen OB1 association, which is located at a mean distance of 2.2 kpc (Kaltcheva & Georgiev 1994). The line of sight towards some of the members of Cen OB1 passes the southern Coalsack, which is located at a mean photometric distance of 175 pc (Rodgers 1960). Note however that the derived distances to various members of Cen OB1 deviate significantly from the mean distance to the association. Examples are HD 114886 (1.3 kpc) and HD 115704 (4.2 kpc) (e.g. Kaltcheva & Georgiev 1994). Westerlund & Garnier (1989) suggested that Cen OB1 may consist of two groups of stars. Because of these ambiguities, NGC 4755 is considered as a separate region, although its stars are members of Cen OB1 (Humphreys 1978).

Table 4a summarizes the measurements towards five stars in NGC 4755, while those towards the other stars in Cen OB1 are given in Tab. 4b. Individual CH^+ and CH spectra are shown

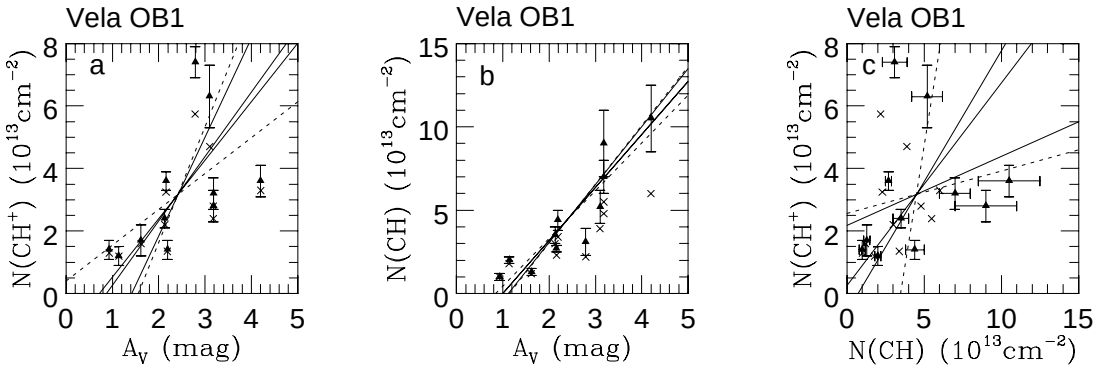

Fig. 6a–c. Vela OB1: Total CH$^+$ and CH column densities plotted versus A_V (**a, b**), and CH$^+$ column densities plotted versus CH column densities (**c**)

in Figs. 7 and 8. Labels 'E' in Fig. 8 mark spectra obtained with EMMI, and the EMMI observations are summarized in Tab 5. The CH$^+$ and CH spectra are characterized by two well resolved absorption lines, with a CH$^+$ line associated with a CH line in general. In NGC 4755 and in Cen OB1, the CH$^+$ and CH velocities agree generally well with each other. Exceptions are HD 111973 and HD 111990 in NGC 4755, which have CH$^+$-CH velocity differences of $\Delta V \approx 3$ km s^{-1} in the blue lines. Towards both stars the corresponding CH$^+$ line is very weak, with a very low line-to continuum ratio. In Cen OB1, the CH$^+$ and CH lines towards HD 115704 indicate a velocity shift of ΔV of 3 and 2 km s^{-1} in the red and blue lines, respectively. There, the CH$^+$ and CH lines are weak, and the absorptions are possibly characterized by more than 2 absorption components. Three other stars, HD 115363, HD 114011, and HD 113432, show a velocity difference of ΔV $\geq$ 2 km s^{-1} in the blue line. HD 114011 has weak and possibly more than 2 CH$^+$ absorption lines, while towards HD 113432, the blue CH absorption line is weak. It is thus likely that most of the velocity differences inferred here are not significant. For the two stars measured in common with the CES and with EMMI, HD 114213 and HD 113432, the equivalent widths agree well with each other, but the inferred radial velocities show large discrepancies, in the 2–6 km s^{-1} range. This is most certainly caused by a well established problem with the entrance window of CCD #34 at the time of the observations. The window suffers from flexure, which may cause jumps and drifts of the location of the spectrum on the CCD in certain ranges of the EMMI position angle of up to 1.5 pixels. (NB EMMI is mounted directly on one adapter of the NTT Nasmyth focus and rotates to compensate for field rotation; the flexure is thus dependent on the observed position).

Figs. 9a,b and 9d,e plot total column densities N(CH$^+$) and N(CH) vs. A_V , for NGC 4755 and Cen OB1, respectively. Although the CH and CH$^+$ absorption lines split into two well resolved components, total column densities are used because it is not clear what fraction of A_V is to be assigned to the individual components. In Figs. 9c and f, individual CH$^+$ and CH column densities inferred from the two absorption components are used, with open and filled symbols corresponding to column densities obtained from the red and blue lines, respectively. Saturation corrections are applied to the individual components. Crosses in Figs. 9a-f represent the column densities not corrected for saturation. Boxes in Figs. 9d,e indicate NGC 4755 stars. In NGC 4755, the increase of N(CH$^+$) and of N(CH) with A_V is clearly established. In Cen OB1, there is a large scatter in the N(CH$^+$)-A_V relation. This may be caused by two sightlines which are characterized by a seemingly low CH$^+$ abundance, HD 114213 and HD 114011. These two stars are located outside the Coalsack region. The other sightlines in Cen OB1 show the general trend of increasing CH$^+$ abundances with increasing visual extinction.

Table 4a. CH$^+$ and CH measurements towards NGC 4755[a]

Star	A_V	λ_{hel}	V_{hel}	W_λ	N_∞	N_b
HD111973	0.99	4232.36	–13.3	3.5(0.5)	0.4(.1)	
		4232.67	8.6	7.5(0.5)	0.9(.1)	
		4300.16	–10.6	2.5(0.5)	0.3(.1)	
		4300.43	8.2	4.5(0.5)	0.5(.1)	
HD111904	1.00	4232.37	–12.6	6.0(0.5)	0.7(.1)	
		4232.67	8.6	4.5(0.5)	0.5(.1)	
		4300.14	–12.0	2.0(0.5)	0.2(.1)	
		4300.43	8.2	3.5(0.5)	0.4(.1)	
HD111934	1.08	4232.38	–11.9	5.0(0.5)	0.6(.1)	
		4232.67	8.6	5.0(0.5)	0.6(.1)	
		4300.16	–10.6	3.5(0.5)	0.4(.1)	
		4300.43	8.2	4.0(0.5)	0.5(.1)	
HD111990	1.17	4232.35	–14.0	8.0(1.0)	0.9(.1)	
		4232.66	7.9	5.0(1.0)	0.6(.1)	
		4300.16	–10.6	3.0(1.0)	0.4(.1)	
		4300.43	8.2	5.5(0.5)	0.7(.1)	
–59°4551	1.40	4232.39	–11.2	14.0(1.0)	1.6(.1)	1.8
		4232.65	7.2	7.5(1.0)	0.9(.1)	
		4300.16	–10.6	5.5(1.0)	0.7(.1)	
		4300.43	8.2	6.0(1.0)	0.7(.1)	

[a] see text for units

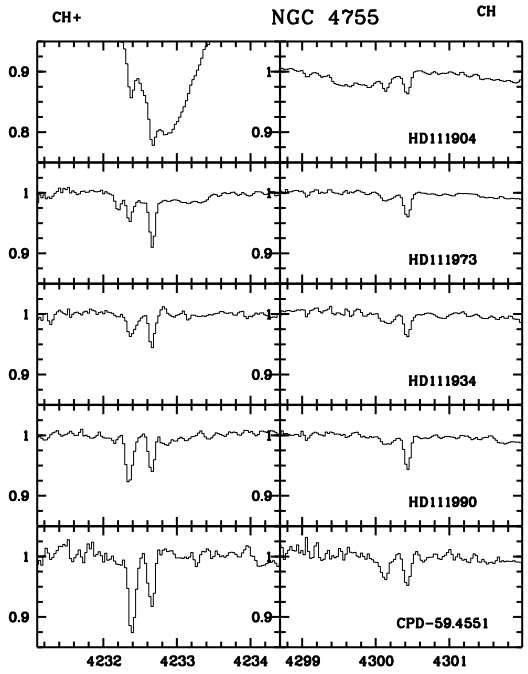

Fig. 7. CH^+ and CH spectra towards individual stars in NGC 4755

4. Discussion

4.1. The CH^+ - CH velocity shift and shock formation of CH^+

From the results presented in Sects. 3.1-3.4 it can be seen that in general, the CH^+ and CH velocities agree within the measurement uncertainties. In the present study, velocity shifts exceeding some 1–2 km s^{-1} are inferred only if the corresponding spectra have a low S/N or if the absorption lines are affected by unresolved velocity components. The absence of a significant velocity shift between CH^+ and CH is further demonstrated in Fig. 10a, where the distribution of the velocity differences as inferred from the CAT observations is shown, per velocity bin of 0.5 km s^{-1} . A single Gaussian fit peaks at 0.2 km s^{-1} . It is characterized by a dispersion of FWHM = 1.5 km s^{-1} which is close to the measurement uncertainties. Fig. 10b contains a plot of the CH^+ column densities as a function of the CH^+-CH velocity shift ΔV. In general, large CH^+ columns occur towards lines of sight where ΔV is small, whereas low CH^+ column densities are associated with large values of ΔV. What Fig. 10b shows is that in the present study, the inferred velocities are more uncertain whenever the line-to-continuum ratio is low. These findings are in contrast with expectations from single shocks. The comprehensive magnetic shock models of Pineau des Forêts et al. (1986) require an increase in shock velocity, and consequently ΔV, for increasing CH^+ columns. Column densities of $N(CH^+) = 1 - 5 \times 10^{13}$ cm^{-2} can be produced in magnetic shocks with speeds in the 8–20 km s^{-1} range. Large columns of CH are produced in the shocked region as well, and N(CH) increases rapidly with the shock speed. The velocity difference between the ions and the neutrals reaches maximal values of $(u_i - u_n)_{max} = 5 - 13$ km s^{-1} for these shocks. The regions where CH and CH^+ prevail are characterized by velocity differences between the ions and the neutrals which reach fractions of 50%–100% of $(u_i - u_n)_{max}$ (Pineau des Forêts et al. 1986). For randomly oriented lines of sight, shifts of several km s^{-1} are thus expected for the CH^+ - CH velocity difference, if the observed CH is entirely produced in the shock. In non-magnetic shocks, shifts of several km s^{-1} between CH^+ and CH are expected as well if CH traces the compressed, post-shock gas (e.g. Lambert & Danks 1986).

The results summarized in Figs. 10a,b are in contrast with those of Allen (1994), who found distinct velocity shifts between CH^+ and CH towards some lines of sight with high CH^+ column densities. As discussed earlier (Sect. 3.1), there are discrepancies towards the one sightline studied in common, HD 54662, where Allen's (1994) value of $\Delta V \approx 4$ km s^{-1} is in contrast with the value of $\Delta V < 1$ km s^{-1} found here. A value of $\Delta V \approx 1$

Table 4b. CH^+ and CH measurements towards Cen OB1[a]

Star	A_V	λ_{hel}	V_{hel}	W_λ	N_∞	N_b
HD114886	1.29	4232.26	–20.4	5.5(0.5)	0.6(.1)	
		4232.58	2.3	11.0(0.5)	1.3(.1)	1.4
		4300.00	–21.8	3.5(0.5)	0.4(.1)	
		4300.37	4.0	4.5(0.5)	0.5(.1)	
HD115704	2.22	4232.18	–26.0	17.5(3.0)	2.0(.3)	2.3
		4232.57	1.6	3.0(1.0)	0.3(.1)	
		3957.38	–23.6	9.5(2.0)	2.1(.4)	2.3
		3957.74	3.7	3.0(1.5)	0.7(.3)	
		4299.91	–28.0	10.5(1.0)	1.3(.1)	
		4300.33	1.2	4.0(1.0)	0.5(.1)	
HD112366	2.25	4232.35	–14.0	9.5(0.5)	1.1(.1)	
		4232.62	5.1	7.0(1.0)	0.8(.1)	
		3957.51	–13.8	7.0(1.5)	1.5(.3)	1.5
		3957.73	2.9	6.5(1.5)	1.4(.3)	1.4
		4300.10	–14:	≤ 3.0	≤ 0.4	
		4300.39	5.4	27.5(1.0)	3.3(.1)	4.3
HD115363	2.58	4232.26	–20.4	8.0(1.5)	0.9(.2)	
		4232.61	4.4	7.5(1.5)	0.9(.2)	
		4299.99	–22.5	9.0(1.0)	1.1(.1)	
		4300.38	4.7	18.0(1.0)	2.2(.1)	2.5
HD110639	2.73	4232.27	–19.6	10.0(0.5)	1.2(.1)	
		4232.61	4.4	18.5(0.5)	2.1(.1)	2.4
		4300.03	–19.7	17.0(2.0)	2.1(.2)	2.3
		4300.38	4.7	12.5(1.0)	1.5(.1)	1.7
HD113432	3.06	4300.06	–17.6	10.0(1.5)	1.2(.2)	1.3
		4300.38	4.7	31.0(1.5)	3.7(.2)	5.0
HD113422	3.24	4232.29	–18.2	28.5(2.0)	3.3(.2)	4.0
		4232.60	3.7	12.5(2.0)	1.4(.2)	1.6
		4300.05	–18.3	23.0(1.0)	2.8(.1)	3.4
		4300.36	3.3	14.0(1.0)	1.7(.1)	2.0
HD112272	3.27	4232.46	–6.2	19.5(1.5)	2.3(.2)	2.5
		4232.65	7.2	8.5(1.5)	1.0(.2)	
		3957.58	–8.5	11.5(1.5)	2.5(.3)	2.7
		3957.75	4.4	8.5(1.5)	1.9(.3)	2.0
		4300.20	–7.9	18.5(1.0)	2.2(.1)	2.7
		4300.37	4.0	20.0(1.0)	2.4(.1)	2.9
HD114213	3.42	4300.04	–19.0	25.5(1.5)	3.1(.2)	3.9
		4300.37	4.0	11.0(1.5)	1.3(.2)	1.5

[a] see text for units

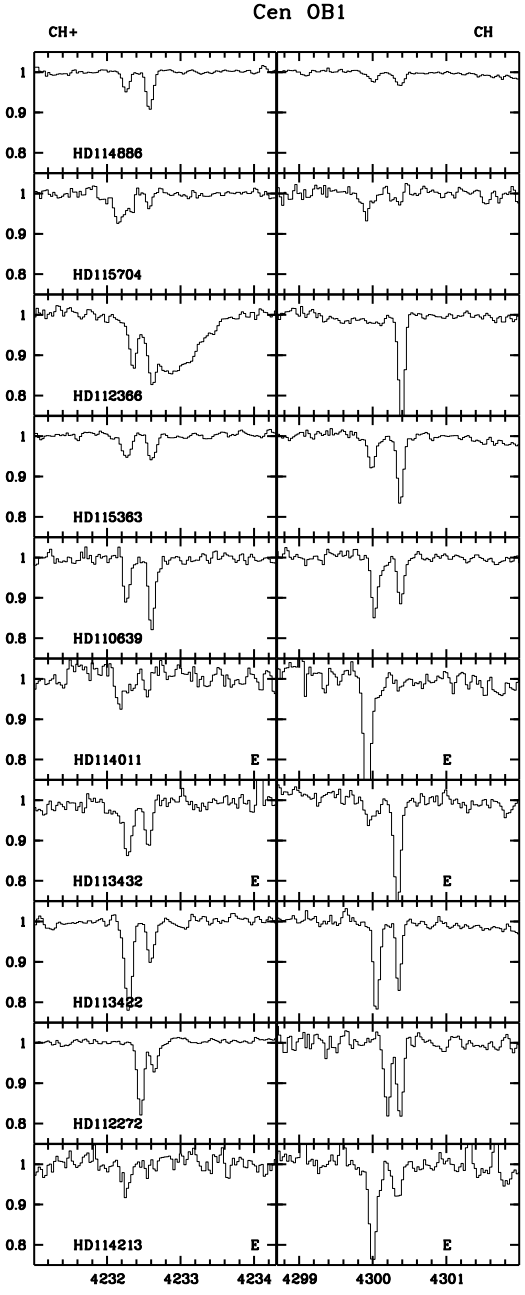

Fig. 8. CH$^+$ and CH spectra towards individual stars in Cen OB1. Labels E identify spectra taken with EMMI

km s^{-1} is also obtained from the data of Danks et al. (1984) and Lambert & Danks (1986), but given the discrepancies in the CH velocities that exist between Danks et al. (1984) and the present study, the agreement in ΔV must be considered fortunate. Other discrepancies exist for two lines of sight measured in common in Allen (1994) and in Gredel et al. (1993). While Allen (1994) found shifts of ΔV = 7 km s^{-1} and 3 km s^{-1} towards HD 53367 and HD 169454, respectively, Gredel et al. (1993) found that the CH$^+$ and the CH velocities towards these two stars agree within the errors. There are discrepancies in the reported line profiles as well. Allen (1994) obtained spectra at R=88000, which is higher than the spectral resolution adopted here or in Gredel et al. (1993), but did not detect some of the weaker features seen here or in Gredel et al. (1993). It is thus speculated that part of the differences in ΔV result from a different S/N in the corresponding spectra.

Table 5. CH$^+$ and CH observations performed with EMMI [a]

Star	A_V	λ_{hel}	V_{hel}	W_λ	N_∞	N_b
–32°1734	3.66	4233.08	37.3	41.5(3.)	4.8(.4)	6.4
		4300.84	36.7	51.5(3.)	6.2(.4)	10
–33°1768	4.38	4233.16	43.3	31.0(3.)	3.6(.4)	4.4
		4300.87	38.6	59.0(3.)	7.1(.4)	15
–44°3129	3.06	4232.87	22.8	41.0(3.)	4.7(.4)	6.3
		4300.62	21.4	32.0(3.)	3.9(.4)	5.2
HD113432	3.06	4232.28	–19.0	17.0(3.)	2.0(.4)	2.2
		4232.56	0.9	11.5(3.)	1.3(.4)	1.4
		4299.98	–23.2	12.0(3.)	1.4(.4)	1.6
		4300.34	1.9	31.0(3.)	3.7(.4)	5.0
HD114011	2.94	4232.21	–23.9	16.0(3.)	1.9(.4)	2.0
		4232.55	0.1	5.0(3.)	0.6(.4)	0.6
		4299.93	–26.6	39.0(3.)	4.7(.4)	7.9
		4300.37	4:	≤ 4	≤ 0.5	≤ 0.5
HD114213	3.42	4232.26	–20.4	11.0(3.)	1.3(.4)	1.3
		4232.56	1:	≤ 4	≤ 0.5	≤ 0.5
		4300.00	–21.8	30.5(3.)	3.7(.4)	4.9
		4300.33	1.5	10.0(3.)	1.2(.4)	1.3

[a] see text for units

Very high resolution observations of Lambert et al. (1990) demonstrated that the CH$^+$-CH velocity difference towards ζ Oph is less than 0.5 km s^{-1} , in disagreement with the value of 2.2 km s^{-1} predicted from the magnetic shock model constructed by Draine (1986) for that line of sight (his model A). Recent observations performed at R$>$ 500000 by Crawford (1995) and by Crane et al. (1995) also find a good agreement between the CH$^+$ and the CH velocities towards the sightlines studied there.

The absence of a significant velocity shift from the present sample together with the absence of a correlation of N(CH$^+$) with the CH$^+$ - CH velocity difference weakens the possibility that magnetic shocks are the general mechanism that produces interstellar CH$^+$. As will be shown in the following section, the CH$^+$ column density is correlated to the visual extinction of the background star. For randomly oriented lines of sight, such a correlation may indicate that sightlines with large values of A_V are affected by multiple shocks, as A_V generally increases with the distance of the background stars. For individual clouds, however, the correlation of N(CH$^+$) to A_V is difficult to reconcile with the shock hypothesis, unless the number of shocks correlates to the optical depth of a cloud.

The MHD shocks produce ubiquitous amounts of CH as well, and both the abundance of CH$^+$ and CH produced in the shock increase with the shock velocity (Pineau des Forêts et al. 1996). Magnetic shocks with speeds of $8-20$ km s^{-1} produce CH columns of $N(\mathrm{CH}) = 2-25\times10^{13}$ cm^{-2} (Pineau des Forêts et al. 1986), which is a major fraction of the CH that is observed here. If magnetic shocks prevail, it is thus expected that N(CH$^+$)

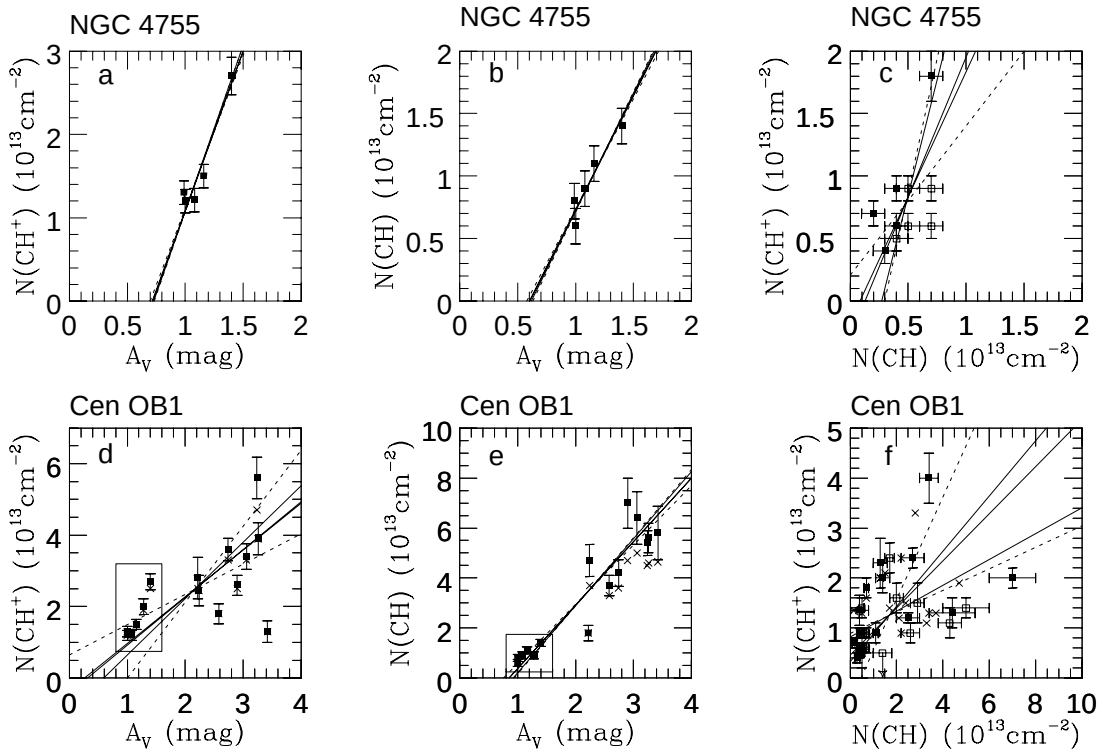

Fig. 9a–f. a-c NGC 4755: Total CH^+ and CH column densities plotted versus A_V (**a, b**), and CH^+ column densities plotted versus CH column densities (**c**). **d-f** Cen OB1: Total CH^+ and CH column densities plotted versus A_V (**d, e**), and CH^+ column densities plotted versus that CH column densities (**f**) The box drawn in **d** and **e** indicates data from NGC 4755. Open and closed symbols in **c** and f correspond to red and blue velocity components, respectively

correlates to N(CH). As shown in Sects. 4.2 and 4.3, such a correlation is indeed established here. However, a very tight correlation of N(CH) to A_V is found as well, which is not expected from the shock models. In translucent molecular clouds, the N(CH) - A_V relation is generally interpreted to reflect the correlation of N(CH) to $N(H_2)$ (Danks et al. 1984, Mattila 1986). The tight correlation between N(CH) and A_V towards any of the regions observed here may thus indicate that only a minor fraction of the observed CH is produced in shocks. This demands weak shocks, with shock speeds $<<$ 10 km s^{-1} . Weak shocks produce only low column densities of CH^+, with $N(CH^+) < 10^{13}$ cm^{-2}, which is not enough to explain the CH^+ column densities observed here. An additional argument against the shock hypothesis is provided by the study of Jenniskens et al. (1992), who found no correlation of the CH^+ column density and the linear rise of the ultraviolet extinction curve.

While the present study provides little evidence that magnetic shocks contribute as the general CH^+ production mechanism, they may nevertheless be at work towards particular sightlines. Examples may include HD 190603 (Allen & Snow 1992) or HD 188220 in DBB36 (Penprase 1993), or other sightlines where significant velocity shifts between CH^+ and CH have been established.

4.2. Linear regressions in CH^+ - A_V , CH - A_V , CH^+ - CH

The diagrams shown in Figs. 2, 4, 6, and 9, contain various linear regression lines which are now discussed. Higher order or multivariate dependencies are not considered. It should be noted that the data presented here do not represent an unbiased sample. All stars were selected to have an apparent magnitude brighter than some 10 mag, which was required to obtain a decent S/N in a reasonable time of observation. A comprehensive discussion on linear regression methods is given in Isobe et al. (1990) and in Feigelson & Babu (1992). The authors provide analytic expressions to calculate ordinary linear regressions of y on x, OLS(x|y), and of the inverse fit of x on y, OLS(y|x), of the bisector of the two OLS lines, and of orthogonal regression and the reduced major axis regression. As explained there in detail, the two OLS methods should not be used; in OLS, the two variables are not treated symmetrically, because it is assumed that only the dependent variable has random error with a constant variance whereas the other variable is errorless. The authors suggest to use either orthogonal regression or the OLS bisector to estimate the linear relation between two variables.

Table 6 contains the intercept coefficients α and the slope β for the various regions studied here. Values of α and β obtained from the five different methods OLS(x|y), OLS(y|x), bisector, orthogonal, and reduced major axis, are given in rows 1–5, respectively, for each region. The estimate of the variance (var)

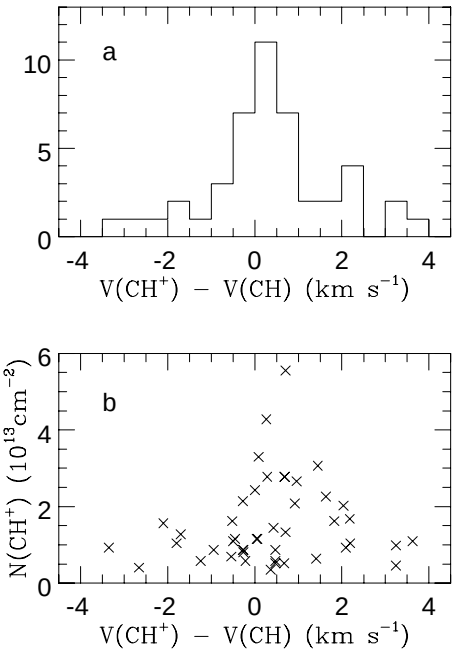

Fig. 10a,b. Distribution of CH$^+$-CH velocity differences, with **a** number of occurrences per bin of 0.5 km s^{-1} , and **b** measured CH$^+$ column densities plotted versus the CH$^+$-CH velocity difference

of both parameters is given in parenthesis and has been calculated employing the expressions listed in Isobe et al. (1990). The corresponding values of the orthogonal regression analysis are emphasized using bold font in Tab. 6. The number of data points N used to calculate the regression coefficients is given as well. Because the absorption lines towards NGC 4755 and Cen OB1 are double, the data set used in the calculation of the N(CH$^+$)-N(CH) correlation is twice as large as that used in the calculation of the N(CH$^+$)-$A_{\rm V}$ and the N(CH)-$A_{\rm V}$ correlations (cf. Sect. 3.4).

A number of conclusions can be drawn from this analysis. First, it is obvious from the values listed in Tab. 6 and the regression lines drawn in Figs. 2, 4, 6, and 9, that the five different methods result in very similar regressions for the N(CH)-$A_{\rm V}$ relation. The fact that this holds for all regions studied here points to a strong correlation of N(CH) to $A_{\rm V}$, as it is expected in translucent clouds (cf. Sect. 4.1). It can also be seen that the inferred slope is significantly different from region to region, with the smallest slope in CMa OB1 and the largest in NGC 2439. Whether this indicates a different functional dependence of N(CH) upon $A_{\rm V}$ is not clear, however. The slope is large whenever the particular region contains lines of sight with high CH column densities. This may suggest that the applied saturation corrections for CH are too large, possibly because the adopted CH Doppler-b value of 1.5 km s^{-1} is too high.

The regression coefficients in the N(CH$^+$)-$A_{\rm V}$ relation are very similar from region to region. This may point to a common and general CH$^+$ formation scenario that prevails in all regions. An exception is NGC 4755, but there the slope is strongly affected by one data point. In addition, the five different regression methods result in similar slopes in CMa OB1, NGC 2439, and NGC 4755, which indicates that N(CH$^+$) is strongly correlated to $A_{\rm V}$. For Vela OB1 and Cen OB1, significantly different slopes result from the various methods, This suggests that the functional dependence of N(CH$^+$) on $A_{\rm V}$ is not as clearly pronounced as it is in the other regions. Note however that in Vela OB1, the variance in the slope is large because HD 75860 and CPD–44°3129 have very high CH$^+$ column densities, whereas in Cen OB1 it is large because HD 114011 and HD 114213 have very low CH$^+$ columns, compared to the values expected from the purported N(CH$^+$)-$A_{\rm V}$ regressions in the two regions. The two sightlines in Cen OB1 do not pass the Coalsack region, and HD 75860 in Vela OB1 is probably associated with the HII region RCW 75. None of these data points is rejected here as outliers or discordant. It may nevertheless be speculated that in Vela, a few sightlines are affected by more than one CH$^+$ formation mechanism, whereas in Cen OB1, the CH$^+$ forming regions are largely associated to the Coalsack.

The regression coefficients obtained for the N(CH$^+$)-N(CH) relation show a large scatter in general. Part of that may be caused by the uncertainties in the CH saturation corrections, as discussed above. As shown in the following section, N(CH$^+$) is nevertheless correlated to N(CH). It is thus concluded that N(CH$^+$) is correlated to N(H$_2$), and consequently to the optical depth of the cloud. It is argued in Sect. 4.4 that the CH$^+$ formation may be driven by the dissipation of turbulence. Turbulence probably occurs at all scales in molecular clouds (e.g. Miesch & Bally 1994), and a correlation of N(CH$^+$) to the total column density of molecular hydrogen may be expected. At the same time, turbulence is a stochastic process. If the formation of CH$^+$ is driven by turbulence, a N(CH$^+$) - N(H$_2$) correlation is expected to show a larger dispersion than say a N(CH)-N(H$_2$) correlation. This is exactly what is observed here, and what is reflected in the regression coefficients listed in Tab. 6.

Fig. 11a-f summarizes all the measurements obtained here. It also includes the data of Gredel et al (1993), which are represented by open symbols. Figs. 10a-c shows column densities inferred in the limit of $b \rightarrow \infty$ (no saturation corrections), while Figs. 10d-f contains the column densities corrected for saturation. The various regression lines correspond to OLS (dashed lines) and to bisector, orthogonal, and reduced major axis (solid lines). The corresponding regression coefficients are given in the last rows of Tab. 6, labeled 'All Data'. It can be seen that there is a general trend that N(CH$^+$) increases with the visual extinction $A_{\rm V}$, and that N(CH$^+$) increases with N(CH). There is a large scatter in the diagram but the probability that N(CH$^+$) is not correlated to N(CH) is less than 0.1% (see following section). As discussed above, a large scatter in the N(CH$^+$)-N(CH) correlation may be expected if the formation of CH$^+$ involves turbulence.

The plot of N(CH$^+$) vs. $A_{\rm V}$ given in Allen (1994), their figure 7, has been interpreted elsewhere to show that N(CH$^+$) is not correlated to $A_{\rm V}$. Allen's (1994) diagram contains the data points measured towards the Pleiades (White 1984a), which all have small values of $A_{\rm V}$ but very high CH$^+$ column densities. It has been argued by White (1984b) that the CH$^+$ in the Pleiades

Table 6. Linear regression coefficients

CH^+ - A_V		CH - A_V		CH^+ - CH	
α (var)	β (var)	α (var)	β (var)	α (var)	β (var)
CMa OB 1 (N=5)					
–0.74 (0.16)	2.10 (0.23)	–0.38 (0.01)	1.04 (0.01)	0.06 (0.02)	1.96 (0.18)
–1.10 (0.19)	2.54 (0.16)	–0.44 (0.02)	1.11 (0.01)	–0.13 (0.03)	2.36 (0.06)
–0.91 (0.17)	**2.30 (0.19)**	**–0.41 (0.01)**	**1.07 (0.01)**	**–0.03 (0.02)**	**2.14 (0.12)**
–1.04 (0.19)	2.47 (0.18)	–0.41 (0.01)	1.08 (0.01)	–0.10 (0.03)	2.29 (0.08)
–0.91 (0.17)	2.31 (0.19)	–0.41 (0.01)	1.07 (0.01)	–0.03 (0.02)	2.15 (0.11)
NGC2439 (N=7)					
–0.58 (1.06)	1.41 (0.16)	–4.14 (1.53)	4.06 (0.19)	1.26 (0.66)	0.29 (0.01)
–2.31 (0.93)	2.04 (0.15)	–4.97 (1.31)	4.36 (0.12)	–0.63 (0.60)	0.56 (0.02)
–1.33 (0.92)	**1.68 (0.15)**	**–4.54 (1.40)**	**4.21 (0.15)**	**0.36 (0.57)**	**0.42 (0.01)**
–1.83 (1.21)	1.86 (0.20)	–4.93 (1.33)	4.35 (0.12)	1.1 (0.80)	0.31 (0.02)
–1.37 (0.93)	1.70 (0.15)	–4.55 (1.39)	4.21 (0.15)	0.47 (0.63)	0.40 (0.01)
Vela OB1 (N=11)					
0.40 (0.54)	1.15 (0.16)	–2.45 (0.63)	2.88 (0.12)	2.57 (0.86)	0.14 (0.01)
–5.82 (12.1)	3.72 (1.95)	–4.03 (1.60)	3.53 (0.20)	–10.8 (235)	3.10 (11.3)
–1.36 (0.71)	**1.88 (0.26)**	**–3.17 (0.85)**	**3.18 (0.12)**	**–0.60 (0.58)**	**0.84 (0.04)**
–4.47 (10.6)	3.16 (1.94)	–3.89 (1.51)	3.47 (0.19)	2.18 (1.01)	0.22 (0.03)
–1.82 (1.31)	2.07 (0.38)	–3.20 (0.88)	3.19 (0.12)	0.26 (0.22)	0.65 (0.04)
NGC 4755 (N=5, 10)					
–2.57 (0.22)	3.68 (0.16)	–1.02 (0.06)	1.76 (0.04)	0.22 (0.09)	1.19 (0.58)
–2.96 (0.15)	4.02 (0.08)	–1.21 (0.12)	1.92 (0.09)	–1.27 (0.34)	4.30 (0.91)
–2.75 (0.17)	**3.84 (0.11)**	**–1.11 (0.08)**	**1.84 (0.06)**	**–0.17 (0.11)**	**2.00 (0.62)**
–2.93 (0.15)	4.00 (0.08)	–1.16 (0.11)	1.88 (0.08)	–1.00 (0.30)	3.72 (0.95)
–2.76 (0.17)	3.85 (0.10)	–1.11 (0.09)	1.84 (0.06)	–0.29 (0.11)	2.26 (0.55)
Cen OB1 (N=15, 30)					
0.65 (0.26)	0.85 (0.10)	–1.79 (0.06)	2.37 (0.03)	0.90 (0.02)	0.22 (0.01)
–2.13 (2.56)	2.13 (0.38)	–2.57 (0.33)	2.73 (0.08)	–0.47 (0.18)	1.02 (0.08)
–0.35 (0.18)	**1.31 (0.06)**	**–2.16 (0.14)**	**2.54 (0.04)**	**0.33 (0.02)**	**0.55 (0.01)**
–0.94 (0.96)	1.58 (0.19)	–2.47 (0.29)	2.68 (0.08)	0.82 (0.02)	0.26 (0.01)
–0.43 (0.24)	1.34 (0.06)	–2.17 (0.15)	2.54 (0.05)	0.47 (0.02)	0.47 (0.02)
All Data (N=53, 72)					
–0.27 (0.10)	1.34 (0.03)	–3.39 (2.46)	3.48 (0.73)	1.19 (0.03)	0.26 (0.00)
–3.12 (0.69)	2.58 (0.11)	–10.30 (16.3)	6.48 (3.33)	–0.10 (0.24)	0.64 (0.04)
–1.34 (0.11)	**1.81 (0.03)**	**–5.85 (5.34)**	**4.55 (1.31)**	**0.59 (0.06)**	**0.43 (0.01)**
–2.41 (0.47)	2.27 (0.08)	–10.0 (16.6)	6.35 (3.40	1.10 (0.04)	0.28 (0.00)
–1.46 (0.13)	1.86 (0.03)	–6.31 (6.36)	4.75 (1.51)	0.69 (0.05)	0.41 (0.01)

is formed in a photon-dominated region (PDR). However, as shown below, a CH^+ formation in PDRs is probably not the general mechanism that is required to explain the interstellar CH^+ abundance. Allen's plot also contains the measurement of Frisch (1972) towards HD 23728, which has the very high CH^+ abundance of 10^{13} cm^{-2} at E_{B-V} = 0.02 mag, but also the very high measurement uncertainty of 100%. If this point is removed as well, together with the Pleiades', Allen's plot does show that in general, $N(CH^+)$ increases with A_V . So do the plots of Crawford (1989), Wallerstein & Gilroy (1992) and Penprase (1993).

4.3. Statistical significance of the correlations

The most widely used indicator of a dependence of a variable Y_i upon X_i, $i = 1, ...N$, is the linear correlation coefficient, given by $r = \sum x_i \times y_i / \sqrt{(\sum x_i^2 \times \sum y_i^2)}$, where the x_i and y_i are the differences of the individual data values from their mean, $x_i = X_i - \bar{x}$. The linear correlation coefficient ranges from -1 to +1, and assumes values of r = 0 for no correlation and r = +1 or $r = -1$ for perfectly well correlated data. However, a correlation coefficient in itself is difficult to interpret, as in general it does not contain information about the statistical significance of the correlation. The significance is tested by calculating the probability p for a random distribution (that is, no correlation) of N measurements to result in a correlation coefficient r' with $r' \geq r$. The probability p is readily obtained

Table 7. Correlation coefficients[a] and statistical significance

CH^+ - A_V		CH - A_V		CH^+ - CH	
r	p	r	p	r	p
CMa OB1 (N=5)					
0.91	0.032	0.97	0.007	0.91	0.032
0.90	**0.037**	**1.00**	**0**	**0.90**	**0.037**
NGC 2439 (N=7)					
0.83	0.020	0.97	< 0.001	0.73	0.065
0.86	**0.014**	**0.96**	$<$ **0.001**	**0.79**	**0.036**
Vela OB1 (N=11)					
0.56	0.076	0.90	< 0.001	0.21	0.54
0.63	**0.038**	**0.93**	$<$ **0.001**	**0.44**	**0.18**
NGC 4755 (N=5,10)					
0.95	0.012	0.95	0.012	0.53	0.12
0.70	**0.19**	**0.90**	**0.037**	**0.22**	**0.54**
Cen OB1 (N=15, 30)					
0.63	0.012	0.93	< 0.001	0.46	0.011
0.63	**0.012**	**0.92**	$<$ **0.001**	**0.58**	$<$ **0.001**
All Data (N=53, 72)					
0.72	< 0.001	0.73	< 0.001	0.64	< 0.001
0.74	$<$ **0.001**	**0.86**	$<$ **0.001**	**0.68**	$<$ **0.001**

[a] Line 1: Pearson's Product Moment Correlation Coefficient
Line 2: Spearman's Rank Correlation Coefficient

via the value $t = r/\sqrt{(1-r^2)}\sqrt{(N-2)}$, which obeys Student's - t distribution in the absence of a correlation. A random distribution is then rejected at the $1-p$ confidence level. If the underlying probability distribution of both variables is normal, Pearson's product moment correlation coefficient r_p may be calculated and compared with r'. The value of r_p is obtained from the formula given in the preceding paragraph. In the present case, however, the underlying probability distributions of the variables X_i and Y_i are not known. This requires to employ non-parametric tests to check for correlations, which is here done using the 'ranks' $R(x_i)$ and $R(y_i)$ of the two variables. Using the ranks, the above expression for r reduces to $r_s = 1 - (6\sum[R(x_i) - R(y_i)])^2)/(N^3 - N)$, which is Spearman's rank correlation coefficient (see e.g. Edgington 1987 for further reading).

Table 7 lists the correlation coefficients r_p and r_s obtained for the five data sets towards CMa OB1, NGC 2439, Vela OB1, NGC 4755, and Cen OB1. Columns 1, 3, and 5 give the correlation coefficients for the $N(CH^+)$-A_V , N(CH)-A_V , and $N(CH^+)$-N(CH) relations, respectively. For each region, the correlation coefficients r_p and r_s are listed in rows 1 and 2, respectively. The values of Spearman's rank correlation coefficient are emphasized in Tab. 7. Columns 2, 4, and 6, list the probabilities p that the correlation coefficients result from random distributions. As in Tab. 6, the number of measurements N used to calculate the correlation coefficients is given as well.

The analysis shows that the CH^+ column densities are correlated to A_V in all regions studied here. The probabilities that $N(CH^+)$ is randomly distributed with respect to A_V are less than 4% in all cases, except for NGC 4755, where this probability reaches 19%. The value of p towards NGC 4755 is severely affected by the discrepancies in the A_V values between Humphreys (1978), Dachs & Kaiser (1984), and Kaltcheva & Georgiev (1994). The uncertainties in A_V do allow for a rank correlation coefficient of r_s = 1 for the $N(CH^+)$-A_V relation in NGC 4755, i.e. perfectly well correlated data. It is one of the main conclusions of the present work that $N(CH^+)$ is correlated to A_V , and that this correlation holds towards all the regions studied here. Table 7 also shows that the N(CH)-A_V correlation is very tight in all regions, with confidence levels exceeding 99% in general, and a confidence level of $> 96\%$ in NGC 4755. In CMa OB1, NGC 2439, and Cen OB1, the CH^+ column densities are correlated to N(CH), with confidence levels exceeding 96%. In Vela OB1 and in NGC 4755, the confidence levels are low, and the data indicate values of 18% and 54% for the probability that $N(CH^+)$ is not correlated to N(CH). The last two rows of Tab. 7 list the correlation coefficients r_s and r_p obtained from the full data set, including the measurements of Gredel et al. (1993). It can be seen that for this sample (of now randomly oriented lines of sight), $N(CH^+)$ is correlated to A_V , at a confidence level exceeding 99.9%. Correlations of N(CH) to A_V and of $N(CH^+)$ to N(CH) are established at confidence levels exceeding 99.9%.

4.4. CH^+ formation scenarios

As discussed in Sect. 4.1, the present study provides little evidence that magnetic shocks are the general and dominant mechanism that is required to produce interstellar CH^+. The following discussion compares the observational results with expectations from alternative CH^+ formation scenarios, such as formation in photon-dominated regions, in turbulent boundary layers, in intermittent dissipation zones of interstellar turbulence in low density regions, and from processes where CH^+ forms in cool clouds via a fraction of fast but non-Maxwellian H_2 or C^+. Other CH^+ formation processes that may contribute columns of several 10^{12}cm^{-3}, such as shock erosion of grain mantles (Duley et al. 1992), are not discussed here.

4.4.1. Photon-dominated regions

Observations of interstellar CH^+ are generally performed towards early type supergiants. This is because bright stars with a featureless continuum are required to identify the CH^+ absorption lines in the first place. If these stars are close to molecular clouds, the CH^+ may arise from photon-dominated regions (PDRs) created by the stellar radiation field. Abundances and column densities of CH^+ in dense PDRs have recently been calculated by Sternberg & Dalgarno (1995). In their model with a cloud density of $n = 10^6$ cm^{-3} and radiation factors of $\chi = 2 \times 10^5$, the CH^+ is produced in the H/HI/H_2 layer at low optical depths and its abundance peaks at values of $A_V \approx 0.5$ mag. Total column densities reach several 10^{13} cm^{-2} and are independent of the total visual extinction of the cloud. Duley et al. (1992) obtained values of $N(CH^+)$ of a few 10^{13} cm^{-2} for densities in the $10^4 - 10^8$ cm^{-2} range and radiation factors of

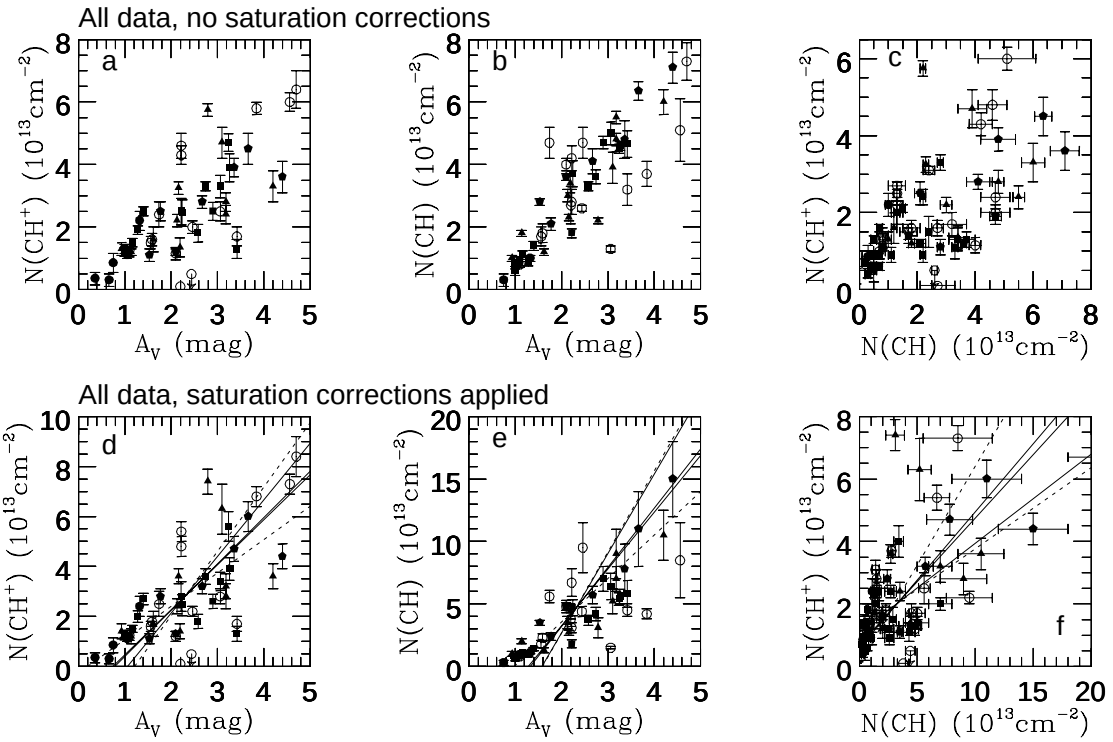

Fig. 11a–f. a-c Plots of CH^+ and CH column density versus visual extinction A_V and of $N(CH^+)$ vs. $N(CH)$, with column densities inferred in the case of $b(CH^+) = b(CH) \rightarrow \infty$. **d-f** As above, except that column densities corrected for saturation effects are used. Dashed and full lines represent various linear regressions fitted to the data - see text

$\chi = 10^3 - 10^6$. As in Sternberg & Dalgarno (1995), the CH^+ abundance peak at the surface of the clouds, at a visual extinction of $A_V << 1$ mag (see e.g. their figure 1). A correlation of $N(CH^+)$ with A_V is thus not expected. The existing models do not include the fact that cloud boundaries are probably fractal (e.g. Falgarone et al. 1991). As pointed out by the referee, it is not clear what the influences of fractal boundaries on the integrated abundances is.

The CH^+ observations towards the Pleiades have been explained earlier by a production of CH^+ in a PDR (White 1984a,b). However, White (1984b) performed an incomplete treatment of the cooling rate (see e.g. Duley et al. 1992) and obtained the heating rates required to form the observed CH^+ column densities at significantly lower values of n and χ, compared to those of Sternberg & Dalgarno (1995). Millimeter CO maps towards sightlines with high CH^+ column densities show that the background stars are associated with translucent clouds (e.g. Gredel et al 1994). Gas densities n towards the clouds inferred from multi-line CO and from C_2 observations range from several hundred to a few 1000 cm^{-3} (e.g. van Dishoeck et al. 1991, Gredel et al. 1993). The densities are orders of magnitude lower than those required in a PDR to produce CH^+. Because of the $N(CH^+)$-A_V correlations and the discrepancy in densities, it can probably be ruled out that PDRs produce the CH^+ that is observed towards OB stars. Exceptions may exist, such as towards BD+31°643. It is the hottest star in the cluster IC 348 and Snow (1993) and Snow et al. (1994) propose that the large column density of interstellar CH^+ observed towards BD+31°643 arises in a PDR. A PDR has also been invoked to explain the circumstellar CH^+ emission that is observed around HD 44179 (Balm & Jura 1992).

4.4.2. Turbulent boundary layers

Duley et al. (1992) investigated the formation of CH^+ in turbulent boundary layers at molecular-cloud—intercloud interfaces. If such boundary layers exist, turbulence may be created by the velocity shear along the interface, and dissipation may create layers of hot gas at the cloud surface. Hartquist & Dyson (1988) and Charnley et al. (1990) suggest that the size of the boundary layer scales with the total thickness of the cloud, and that they have typical depths of a few percent of the dimension of the cloud. Duley et al. (1992) performed calculations for clouds with gas densities in the $n = 60 - 600$ cm^{-3} range, temperatures between T=700–4000 K, and radiation factors of χ=0.3–20, and obtained CH^+ columns of several 10^{13} cm^{-2} for boundary layers of a few 0.1 pc thickness. Hartquist et al. (1992) have used the models to explain the observations of CH^+ towards ζ Oph by Crane et al. (1991).

Turbulent boundary layers fail to produce very high CH^+ column densities of $N(CH^+) >> 10^{13}$ cm^{-2}, unless multiple or intercepting layers occur (Duley et al. 1992). In such a case, the CH^+ absorption lines should break up into multiple velocity components. At the spectral resolution employed here, the

strongest CH^+ absorption lines are dominated by single absorption components in general. In their observations at very high spectral resolution, Crane et al. (1995) found CH^+ columns exceeding 3×10^{13} cm^{-2} in single CH^+ velocity components, in a sample of stars with $A_V \leq 2$ mag. The models of Duley et al. (1992) predict a pronounced increase of the CH^+ abundance with the gas density n, in contrast with the trend of decreasing CH^+ column density with n (Gredel et al. 1993). Turbulent boundary layers thicken with the total depth of a cloud. $N(CH^+)$ is thus expected to correlate with N(CH), which is what is observed here. However, the depths in the boundary layers would have to reach depths up to 10^{18} cm to explain the observed CH^+ columns (e.g. Duley et al. 1992). The energetics required to maintain such regions at several 1000 K are probably too high, as discussed in e.g. Gredel et al. (1993). The existence of the warm H I phase in the Galaxy altogether has recently been questioned by Falgarone & Puget (1995). The authors propose an alternative scenario, and suggest that most of the H I emission arises from a net of small structures at 10^3 K, created by the intermittent dissipation of interstellar turbulence.

4.4.3. Intermittent dissipation zones of interstellar turbulence

In a recent series of papers, Falgarone and coworkers provided strong evidence for the existence of intermittent turbulence in the interstellar medium (e.g. Falgarone & Phillips 1990, Falgarone & Puget 1995). The intermittent dissipation bursts of turbulence create hot layers of material in the interstellar gas. In order to model the effects of the turbulent heating on the chemistry of the clouds, Falgarone et al. (1995) introduce thin layers (depths $\delta\ A_V$ = 0.05 mag) at elevated temperatures (T$>$ 1000 K) in low-density, mostly atomic clouds. The CH^+ which is produced in the hot regions relaxes back to low values after some 10^3 years, which is the time scale at which thermal balance is reached again after the temperature has been transiently elevated. The authors use the results of laboratory measurements to obtain the probability distribution of the dissipation rate. The laboratory measurements were obtained from incompressible fluids without magnetic fields but Falgarone et al. (1995) provide arguments that these rates may be scaled to the interstellar medium.

The models of Falgarone et al. (1995) readily reproduce the CH^+ column densities that are observed in the interstellar medium. However, Falgarone et al. (1995) constrained their models to low-density and mostly atomic clouds, possibly because Falgarone & Puget (1995) suggest that the dissipation of turbulence in the interior of dense molecular clouds does not result in a considerable temperature enhancement (e.g. Fig. 4 of Falgarone & Puget 1995). In addition, the abundance of CH^+ that is produced in the hot layer is largely related to the strength of the dissipation burst. For these two reasons, a correlation of $N(CH^+)$ to A_V and to N(CH) is not expected, as emphasized by Falgarone et al. (1995). This is in conflict with the present observations. However, as pointed out by the referee, the heating and cooling rates used in Falgarone & Puget (1995) are probably rather crude. It is thus not clear if intermittent dissipation bursts can create hot parcels of gas in the deeper interiors of translucent clouds as well. If so, correlations of $N(CH^+)$ to A_V and to N(CH) may very well be expected.

4.4.4. Non-Maxwellian velocity distributions

It was speculated by Gredel et al. (1993) that a fraction of translationally hot H_2 or C^+ may be created in cool clouds via the general interstellar turbulence, such as the dissipation of Alfvén waves. Their estimate to the CH^+ formation rate from the non-Maxwellian velocity distributions resulted in CH^+ abundances somewhat below the observed values. A sophisticated calculation of the velocity distribution which results from the turbulent cascade has recently been performed by Spaans (1995). The author employed the 'Random Beta Model' of Mandelbrot to calculate the probability distribution of the velocity increments on the various scales. The CH^+ formation rate is then calculated in a straightforward manner by folding the velocity increments with the collisional cross sections. Assuming that CH^+ is removed by reactions with H_2 at a rate of 1.2×10^{-9} cm^{3}s^{-1}, Spaans (1995) showed that the CH^+ formation rate which is required to maintain the abundance ratio of $< N(CH^+)/N(H_2) \approx 4 \times 10^{-8}$ (Gredel et al. 1993) is readily obtained in clouds with kinetic temperatures around 50 K, densities ranging from 100–2000 cm^{-3}, and turbulent velocities ranging from 1–4 km s^{-1} , viz. parameters that are considered typical for translucent clouds.

The predictions from Spaans' model are in agreement with observed properties of interstellar CH^+. The model derives a correlation of $N(CH^+)$ with rotationally excited H_2, it predicts that the CH^+-CH velocity shift is small in general although different from zero, and that $N(CH^+)$ increases with decreasing gas density n. If the CH^+ production is driven by the dissipation of turbulence, and if turbulence occurs on all scales, as suggested by e.g. Miesch & Bally (1994), correlations of $N(CH^+)$ to A_V and to N(CH) are expected, because the site of the CH^+ production is not exclusively constrained to a particular region of a cloud such as its surface. The larger scatter in the $N(CH^+)$-A_V and $N(CH^+)$-N(CH) diagrams that is observed here, compared to the tight N(CH)-A_V regression, may reflect the more stochastic nature of the CH^+ formation process, compared to that of CH.

5. Conclusions

From observations of interstellar CH^+ and CH absorption lines towards the southern OB associations CMa OB1, NGC 2439, Vela OB1, NGC 4755 and Cen OB1, the following conclusions are drawn:

1. Towards a particular association, the CH^+ column densities are correlated to the visual extinction of the background stars, and $N(CH^+)$ is correlated to N(CH).
2. In general, the CH^+ and CH radial velocities agree within the measurement uncertainties. The CH^+ column density is not correlated to the CH^+-CH velocity difference.
3. The observations provide little evidence that a CH^+ production in magnetic shocks is the general formation mechanism

that is required to explain the ubiquitous abundance of CH^+ in the interstellar medium.

4. It is difficult to reconcile the present observations with a CH^+ production mechanism that is constrained to the surface of the clouds, such as formation in photon-dominated regions.
5. The observations support CH^+ formation scenarios which involve the dissipation of interstellar turbulence. In particular, the observed column densities of CH^+ and the correlations of $N(CH^+)$ to A_V and to $N(CH)$ are expected from a model where the endothermic reaction that produces CH^+ is driven by a fraction of translationally hot H_2 or C^+, created via the dissipation of interstellar turbulence.

Acknowledgements. It is a pleasure to thank G. Pineau des Forêts and M. Elitzur for encouraging discussions and comments to improve the paper.

References

Allen, M.M. 1994, ApJ 424, 754
Allen, M.M., Snow, T.P. 1992, ApJ 391, 152
Balm, S.P., Jura, M. 1992, A&A 261, L28
Banse, K., Crane, P., Ounnas, C., Ponz, D. 1983, 'MIDAS', in Proc. of DECUS, Zurich, P. 87
Charnley, S.B., Dyson, J.E., Hartquist, T.W., Williams, D.A. 1990, MNRAS 243, 405
Clariá, J.J. 1974, A&A 37, 229
Crane, P., Hegyi, D.J., Lambert, D.L. 1991, ApJ 378, 181
Crane, P., Lambert, D.L, Sheffer, Y. 1995, ApJS 99, 107
Crawford, I.A. 1989, MNRAS 241, 575
Crawford, I.A. 1995, MNRAS 277, 458
Dachs, J., Kaiser, D. 1984, A&AS 59, 368
Danks, A.C., Federman, S.R., & Lambert, D.L. 1984, A&A 130, 62
Danks, A.C., Sembach, K.R. 1995, AJ 109, 2627
van Dishoeck, E.F., Black, J.H. 1989, ApJ 340, 273
van Dishoeck, E.F., Black, J.H., Phillips, T.G., Gredel, R., 1991, ApJ 366, 141
Draine, B.T. 1986, ApJ 310, 408
Duley, W.W., Hartquist, T.W., Sternberg, A., Wagenblast, R., Williams, D.A. 1992, MNRAS 255, 463
Edgington, E.S., *Randomization Tests*, Marcel Dekker Inc, New York and Basel, 1987
Eggen, O.J. 1980, ApJ 238, 627
Eggen, O.J. 1982, ApJS 50, 199
Elitzur, M., & Watson, W.D. 1978, ApJ 222, L141
Elitzur, M., & Watson, W.D. 1980, ApJ 236, 172
Falgarone, E., Phillips, T.G., 1990, ApJ 359, 344
Falgarone, E., Phillips, T.G., Walker, C.K., 1991, ApJ 378, 186
Falgarone, E., Pineau des Forêts, G., Roueff, E. 1995, A&A 300, 870
Falgarone, E., Puget, J.-L. 1995, A&A 293, 840
Federman, S.R., Strom, C.J., Lambert, D.L., Cardelli, J.A., Smith, V.V., Joseph, C.L. 1994, ApJ 424, 772
Feigelson, E.D., Babu, G.J. 1992, ApJ 397, 55
Frisch, P. 1972, ApJ 173, 301
Gredel, R., van Dishoeck, E.F., Black, J.H. 1991, A&A 251, 625
Gredel, R., van Dishoeck, E.F., Black, J.H. 1993, A&A 269, 477
Gredel, R., van Dishoeck, E.F., Black, J.H. 1994, A&A 285, 300
Hartquist, T.W., Dyson, J.E. 1988, Astrophys. Space Sci. 144, 615
Hartquist, T.W., Dyson, J.E., Williams, D.A. 1992, MNRAS 257, 419
Hawkins, I., Craig, N. 1991, ApJ 375, 642
Humphreys, R.M. 1978, ApJS 38, 309
Isobe, T., Feigelson, E.D., Akritas, M.G., Babu, G.J. 1990, ApJ 364, 104
Jenkins, E.B., Wallerstein, G. 1995, ApJ 440, 227
Jenkins, E.B., Wallerstein, G., Silk, J. 1984, ApJ 278, 649
Jenniskens, P., Ehrenfreund, P., Désert, F.-X. 1992, A&A 265, L1
Kaltcheva, N.T., Georgiev, L.N. 1994, MNRAS 269, 289
Lambert, D.L., Sheffer, Y., & Crane, P. 1990, ApJ 359, L19
Lambert, D.L., Danks, A.C. 1986, ApJ 303, 401
Mattila, K. 1986, A&A 160, 157
Meyer, D.M., Savage, B.D. 1981, ApJ 248, 545
Miesch, M.S., Bally, J. 1994, ApJ 429, 645
Murphy, D.C., May, J. 1991, A&A 247, 202
Nakano, M., Yoshida, S., Kogure, T. 1984, PASJ 36, 517
Penprase, B.E. 1993, ApJS 88, 433
Pineau des Forêts, G., Flower, D.R., Hartquist, T.W., Dalgarno, A. 1986, MNRAS 220, 801
Rodgers, A.W. 1960, MNRAS 120, 163
Scalo, J. 1990, in *Physical Processes in Fragmentation and Star Formation*, eds. R. Capuzzo-Dolcetta, C. Chiosi, and A. di Fazio, Kluwer Academic Publishers, Dordrecht, p. 151
Slawson, R.W., Reed, B.C. 1988, AJ 96, 988
Snow, T.P. 1993, ApJ 402, L73
Snow, T.P., Hanson, M.M., Seab, C.G., Saken, J.M. 1994, ApJ 420, 632
Spaans, M. *Models of Inhomogeneous Interstellar Clouds*, Ph.D. thesis, Leiden 1995
Sternberg, A., Dalgarno, A. 1995, ApJS 99, 565
Turner, D.G. 1977, AJ 82, 805
Wallerstein, G., Vanture, A., Jenkins, E.B. 1995, ApJ 455, 590
Wallerstein, G., Balick, B. 1990, MNRAS 245, 701
Wallerstein, G., Gilroy, K. K. 1992, AJ 103, 1346
Wallerstein, G., Silk, J. 1971, ApJ 170, 289
Westerlund, B.E., Garnier, R. 1989, A&AS 78, 203
White, S.D.M. 1975, ApJ 197, 67
White, R.E. 1984a, ApJ 284, 685
White, R.E. 1984b, ApJ 284, 695
Williams, D.A. 1992, Planet. Space Sci. 40, 1683

This article was processed by the author using Springer-Verlag LaTeX A&A style file *L-AA* version 3.